

Low-frequency Acoustic Collimation Modulation Based on Monopole Mie Resonance Acoustic Metamaterials

Bo Zheng^{1, 2, 3, a}, Zigeng Liu^{1, 2, 3, b}, Ang Li^{1, 2, 3, c}, Botao Liu^{1, 2, 3, d},
Junda Shen^{1, 2, 3, e}, and Shengchun Liu^{1, 2, 3, f, *}

¹National Key Laboratory of Underwater Acoustic Technology, Harbin Engineering University, Harbin 150001, China;

²Key Laboratory of Marine Information Acquisition and Security (Harbin Engineering University), Ministry of Industry and Information Technology, Harbin 150001, China;

³College of Underwater Acoustic Engineering, Harbin Engineering University, Harbin 150001, China.

^abozheng@hrbeu.edu.cn, ^bliuzg@hrbeu.edu.cn, ^cleeang58@hrbeu.edu.cn,

^dliubotao@hrbeu.edu.cn, ^eshenjunda1998@hrbeu.edu.cn, ^{f, *}lsc@hrbeu.edu.cn

Abstract. Acoustic metamaterials show great flexibility in manipulating acoustic waves and exhibit important applications. However, an increasing number of applications are suitable for the low-frequency range, which makes it challenging to design acoustic metamaterials for low-frequency modulation. Here, we propose a subwavelength monopole Mie resonance acoustic metamaterial that can flexibly control the propagation route of acoustic waves. Compared to the background medium, the designed Mie unit has a higher refractive index and can achieve directional manipulation of low-frequency acoustic waves based on monopole Mie resonance. Furthermore, an array formed by multiple Mie units in a specific arrangement can achieve the acoustic collimation phenomenon. The designed monopole Mie resonance acoustic metamaterial has potential application prospects in fields such as low-frequency filtering, noise suppression, and nondestructive testing.

Keywords: Mie resonance; acoustic metamaterials; low-frequency acoustic manipulation; acoustic collimation.

1. Introduction

In a homogeneous medium, acoustic waves exhibit a clear divergence trend during propagation due to the diffraction effect. However, this phenomenon of acoustic divergence is not suitable for practical applications. To satisfy specific requirements, selecting appropriate radiation methods can not only effectively save the energy of transmitted acoustic waves but also provide protection for acoustic signals. In previous studies, traditional methods for directional radiation mainly relied on adjusting the acoustic source, such as phase arrays [1]. However, the traditional method has some drawbacks, such as the large size of loudspeaker arrays and the expensive price, which are not favorable to engineering practice. Phononic crystals are artificial structures with periodic layouts that provide a new method for realizing acoustic radiation modulation by utilizing their properties such as anisotropy [2, 3], antiresonance [4, 5], diffraction [6, 7], and band-edge state [8, 9, 10]. However, phononic crystals have certain restrictions due to their size and scattering effects, which limit their application in the low-frequency range.

Acoustic metamaterials can effectively modulate and change the propagation properties of acoustic waves and have made remarkable achievements in the field of wave manipulation, including acoustic cloaking [11, 12], negative refraction [13, 14], acoustic focusing [15, 16, 17], and asymmetric transmission [18, 19]. However, traditional acoustic metamaterials have problems such as high loss, complex structural design, and limited specific properties, which make the design of acoustic metamaterials still need improvement. How to effectively modulate the propagation of low-frequency acoustic waves through subwavelength structures has become a hot issue in current

acoustic research. Quan et al. proposed a cascade-based Helmholtz resonator realizing dipole-like radiation with directivity to miniaturize and integrate acoustic devices [20]. Cheng et al. proposed a highly symmetric folded space to construct an ultraslow-fluid-like structure to realize the Mie resonance phenomenon of low-frequency acoustic waves [21]. Since then, related works based on the Mie resonance have been reported, such as directional sensing [22], rainbow trapping for low-frequency acoustic waves [23], extraordinary acoustic transmission [24], and the reversed Doppler effect [25].

In this paper, we propose a monopole Mie resonance acoustic metamaterial that can modulate acoustic wave radiation in the low-frequency scope. The effects of channel widths and rigid wall thicknesses on the resonance frequency and acoustic field modulation are explored by analyzing the Mie structural parameters. In addition, by constructing two sets of axisymmetric arrays, each containing two Mie units, the acoustic collimation phenomenon is successfully achieved. Furthermore, the effect of the spatial angle between the Mie array and the acoustic source array on the acoustic collimation phenomenon is analyzed. The novel monopole Mie resonance acoustic metamaterial is expected to have far-reaching implications in practical areas such as noise suppression, low-frequency filtering, and nondestructive testing.

2. Theoretical Method

The three-dimensional model diagram of the monopole Mie resonance acoustic metamaterial is shown in Fig. 1(a), and its cross-section diagram in the xy plane is shown in Fig. 1(b), divided into eight equally folded transmission channels. The Mie unit has an outer radius of R , an inner radius of r_1 , a channel width of w , a rigid wall thickness of t , and a space fold number of N within each channel. With the center point O of the Mie unit as the coordinate origin, the actual propagation path from point A to point O in the 90° direction is shown by the red dashed line in Fig. 1(b). The actual propagation path of acoustic waves in the folded channel is elongated rather than a straight distance of AO . The Mie unit has a lower equivalent sound velocity than air. When the refractive index of the Mie unit is higher than the background, Mie resonance modes can be stimulated in the medium. To better analyze the acoustic scattering characteristics of Mie units, a simplified model of folded space is shown in Fig. 1(c). The yellow slit area represents the ultraslow medium. The blue fan-shaped area represents the rigid medium. The white circular area is air. The effective refractive index of the acoustic transmission channel can be expressed as [26]

$$n = \frac{L}{R - r_1} \quad (1)$$

where L is actual propagation distance of sound in the folded channel, which can be written as

$$L = \sum_{n_i=1}^N 2\pi T[r_1 + n_i(t + w) - w] - Nw \quad (2)$$

where T represents the sector ratio. The periodic subwavelength yellow slit region can be equivalent to a uniform material [21], and its equivalent model is separated into three parts, as shown in Fig. 1(d), which are the air layer $r < r_1$, the high refractive index layer $r_1 < r < r_2$, and the virtual layer $r_2 < r < R$. $r_2 = r_1 + (R - r_1)\eta$, $\eta = 8w/2\pi R$ is the filling rate of the channel. The purpose of introducing virtual layers is to maintain the same radius of the equivalent model as the Mie unit. Set $\mathbf{r} = (x, y) = (r, \theta)$, the sound pressure field distribution of the system satisfies the two-dimensional Helmholtz equation

$$(\nabla^2 + k^2)P = 0 \quad (3)$$

The incident and scattering wave components can be expressed in terms of the Bessel function J_m and the Hankel function H_m . The sound pressure field distribution in the whole space can be expressed as [20]

$$P(r) = \begin{cases} \sum_m A_m J_m(k_0 r) e^{im\theta}, & r < r_1 \\ \sum_m [B_m J_m(k_1 r) + C_m H_m(k_1 r)] e^{im\theta}, & r_1 < r < r_2 \\ \sum_m [D_m J_m(k_0 r) + E_m H_m(k_0 r)] e^{im\theta}, & r > R \end{cases} \quad (4)$$

where A_m-E_m is the m -order expansion coefficient for separately layer. k_0 and k_1 are the wave numbers in air and in the equivalent homogeneous medium. When $m = 0$, the monopole resonance frequency can be expressed as

$$f \approx \frac{c_0}{\pi n} \sqrt{\frac{2\eta}{r_1(R-r_1)}} \quad (5)$$

where c_0 is the airborne sound speed.

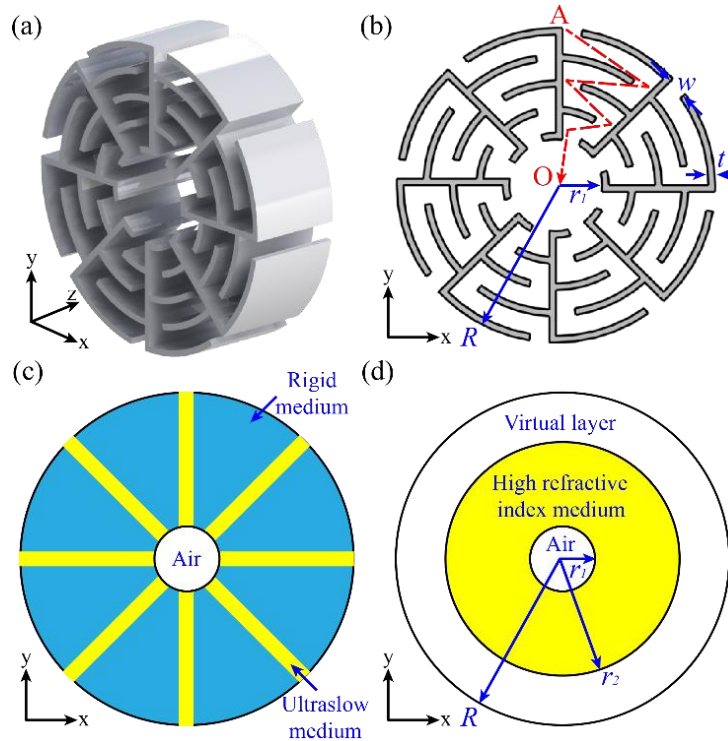


Fig. 1 Mie resonance acoustic metamaterial. (a) Three-dimensional model diagram of the designed Mie unit. (b) Schematic cross-section of the Mie unit in the xy plane. (c) Simplified physical model of a multichannel resonant unit. (d) Equivalent physical model of (c).

3. Results and Discussion

Figure 2(a) displays the distribution of the sound pressure field near the Mie unit at the monopole resonance frequency. The Mie unit is in the monopole resonance mode at the incident frequency of 776 Hz, and the sound pressure field in the inner region is markedly improved. The sound pressure value at the center of the Mie unit reaches the maximum value of 6.64 Pa, which is significantly higher than the sound pressure value of the incident plane wave. In the traditional acoustic monopole resonance state, the structural radius will periodically expand and contract with vibration, while the Mie unit can maintain its radius unchanged. Figure 2(b) shows the phase distribution inside the Mie unit under monopole resonance. In the state of monopole resonance, acoustic waves maintain in-phase vibration inside the Mie unit, and the phase of acoustic waves in all directions is almost the same.

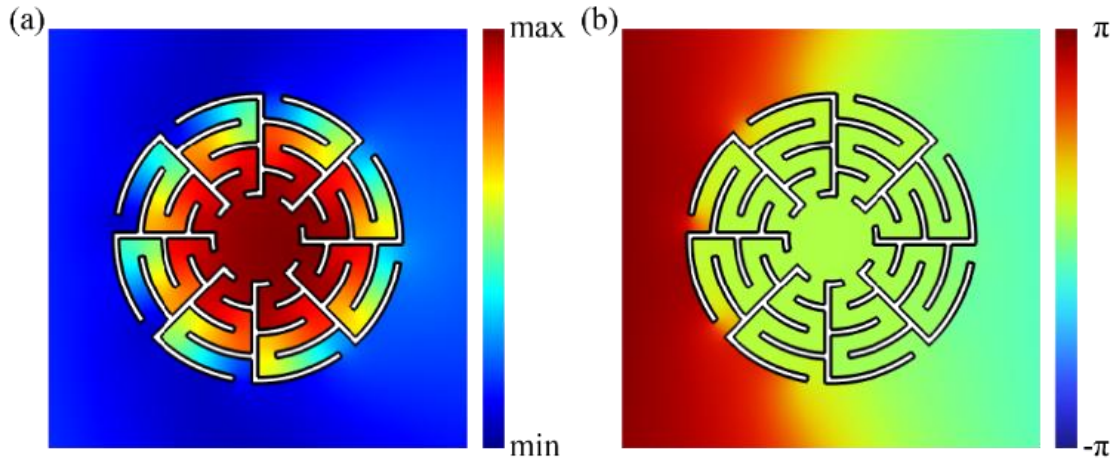


Fig. 2 Monopole Mie resonance metamaterial unit when the incident frequency is 776 Hz (a) Sound pressure field distribution. (b) Phase distribution.

Based on the particularity of the Mie unit, we explore the effects of parameters such as channel width and rigid wall thickness on the resonance frequency and sound pressure field of monopoles. The resonance frequency of the Mie unit is related to the proportion of folding space. Firstly, we discuss the variation of rigid wall thickness t and the modulation of sound field by the Mie unit when the channel width w is constant. The range of variation for the rigid wall thickness t is 1-3 mm. The sound pressure value at the center of the Mie unit varies with frequency, as shown in Fig. 3(a). As the parameter t value increases, the sound pressure value at the center of the Mie unit gradually increases from 5.86 Pa to 7.3 Pa. The monopole resonance frequency of the Mie unit decreases from 850 Hz to 715 Hz, shifting towards lower frequencies. Secondly, we discuss the variation of channel width w and the modulation of the sound field by the Mie unit when the rigid wall thickness t is constant. The variation range of channel width w is between 5-7 mm. The sound pressure value at the center of the Mie unit varies with frequency, as shown in Fig. 3(b). As the parameter w increases, the sound pressure value at the center of the Mie unit gradually decreases from 7.6 Pa to 5.89 Pa. The monopole resonance frequency of the Mie unit decreases from 800 Hz to 745 Hz, shifting towards lower frequencies. It can be concluded that the corresponding changes in parameters t and w will affect the sound pressure value and monopole resonance frequency at the center of the Mie unit.

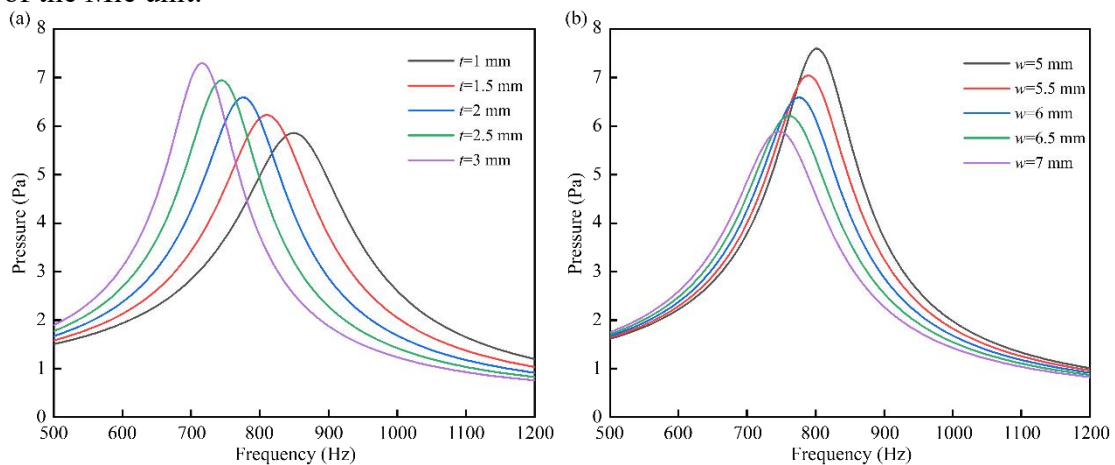


Fig. 3 The effects of channel width and rigid wall thickness on the resonance frequency and sound pressure field of the Mie unit. (a) w is a constant value and t is a variable value. (b) t is a constant value and w is a variable value.

To further explore related applications, we construct a Mie array to achieve a feasible method of acoustic collimation. A single Mie unit only achieves directional scattering in a narrow frequency

range. The narrow frequency band cannot satisfy the actual requirements of people, so we utilize multiple Mie units to form an array to achieve acoustic collimation in a wide frequency range of 750 Hz- 1120 Hz. The schematic diagram of the Mie array is shown in Fig. 4(a), where the distance between two symmetrically placed Mie arrays is a and the angle between the Mie array and planar sound source is θ . The radiation sound field of the Mie array at 776 Hz is shown in Fig. 4(b), where $a = 40$ cm and $\theta = 45^\circ$. The Mie array has a significant control effect on the acoustic wave, limiting the propagation of the acoustic wave along the x -axis direction and ensuring a good collimation effect in the y -axis direction. To explore the effect of parameter θ on acoustic collimation, Figures 4(c) and 4(d) show the radiation sound field of the Mie array when $\theta = 30^\circ$ and $\theta = 60^\circ$, respectively. Comparative analysis of Figs. 4(b)-4(d) shows that when the angle θ becomes smaller, the acoustic collimation effect becomes more convergent, but the sound field intensity decreases. Moreover, more obvious sidelobes appeared, resulting in poor directivity and a shorter acoustic collimation range along the y -axis. When the angle θ becomes larger, the acoustic collimation effect becomes more divergent, but the sound field intensity increases significantly. And the acoustic collimation range along the y -axis becomes longer, which is also accompanied by a small range of sidelobe areas. Therefore, the method of obtaining acoustic collimation with Mie arrays has many advantages. The structural size of the Mie unit is smaller than the working wavelength and can achieve acoustic collimation in a wide frequency range. Compared with sound sources that are difficult to move, the designed Mie unit is more portable because of its small size, providing a new method for changing the target direction.

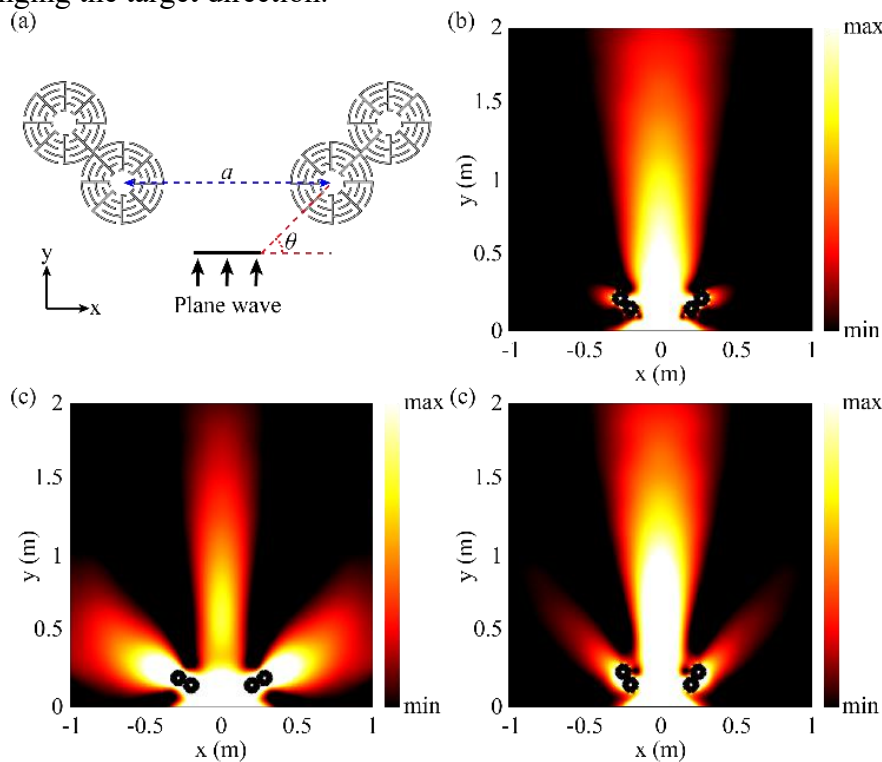


Fig. 4 Acoustic collimation phenomenon via Mie array. (a) The schematic diagram of the Mie array. (b) $a = 40$ cm and $\theta = 45^\circ$, the field intensity distribution of acoustic collimation. (c) $a = 40$ cm and $\theta = 30^\circ$, the field intensity distribution of acoustic collimation. (d) $a = 40$ cm and $\theta = 60^\circ$, the field intensity distribution of acoustic collimation.

4. Summary

In summary, we propose a subwavelength monopole Mie resonance acoustic metamaterial to achieve acoustic radiation directivity modulation. The scattering field of low-frequency acoustic waves can be effectively modulated by utilizing the monopole resonance modes excited by the Mie unit. By changing the rigid wall thickness and channel width of the Mie unit, the impact on the

monopole resonance frequency and sound pressure field is analyzed to provide a basis for subsequent Mie structure optimization. Furthermore, a Mie array is designed to realize the acoustic collimation phenomenon. The planar acoustic wave propagates collimated in the y -axis direction under the control of the Mie array. By changing the angle between the Mie array and planar sound source, the impact of the Mie array location on acoustic collimation control is explored. The designed monopole Mie resonance acoustic metamaterials may have a certain application prospect in noise control and nondestructive testing.

References

- [1] Durnin J., Miceli J. J., and Eberly J. H. Diffraction-Free Beams. *Physical Review Applied*, 1987, 58(15): 1499-1501.
- [2] Pérez-Arjona I., Sánchez-Morcillo V. J., Redondo J., Espinosa V., and Staliunas K. Theoretical prediction of the nondiffractive propagation of sonic waves through periodic acoustic media. *Physical Review B*, 2007, 75(1): 014304.
- [3] Li Bo, Deng Ke, and Zhao Heping. Acoustic guiding and subwavelength imaging with sharp bending by sonic crystal. *Applied Physics Letters*, 2011, 99(5): 051908.
- [4] Han Haoxue, Potyomina L. G., Darinskii A. A., Volz S., and Kosevich Y. A. Phonon interference and thermal conductance reduction in atomic-scale metamaterials. *Physical Review B*, 2014, 89(18): 180301.
- [5] Han Haoxue, Li Baowen, Volz S., and Kosevich Y. A. Ultracompact Interference Phonon Nanocapacitor for Storage and Lasing of Coherent Terahertz Lattice Waves. *Physical Review Letters*, 2015, 114(14): 145501.
- [6] Moiseyenko R. P., Liu J., Declercq N. F., and Laude V. Blazed phononic crystal grating. *Applied Physics Letters*, 2013, 102(3): 034108.
- [7] Moiseyenko R. P., Herbison S., Declercq N. F., and Laude V. Phononic crystal diffraction gratings. *Journal of Applied Physics*, 2012, 111(3): 034907.
- [8] Qiu Chunyin and Liu Zhengyou. Acoustic directional radiation and enhancement caused by band-edge states of two-dimensional phononic crystals. *Applied Physics Letters*, 2006, 89(6): 063106.
- [9] Ke Manzhu, et al. Experimental demonstration of directional acoustic radiation based on two-dimensional phononic crystal band edge states. *Applied Physics Letters*, 2007, 90(8): 083509.
- [10] Soliveres E., Espinosa, V., Perezarjona I., Sanchezmorcillo V. J., and Staliunas K. Self collimation of ultrasound in a three-dimensional sonic crystal. *Applied Physics Letters*, 2009, 94(16): 164101.
- [11] Zhu Xuefeng, Liang Bin, Kan Weiwei, Zou Xinye, and Cheng Jiangchun. Acoustic Cloaking by a Superlens with Single-Negative Materials. *Applied Physics Letters*, 2011, 106(1): 014301.
- [12] Zigoneanu L., Popa B. I., and Cummer S. A. Three-dimensional broadband omnidirectional acoustic ground cloak. *Nature Materials*, 2014, 13: 352-355.
- [13] Brunet T., et al. Soft 3D acoustic metamaterial with negative index. *Nature Materials*, 2015, 14: 384-388.
- [14] Xie Yangbo, Popa B. I., Zigoneanu L., and Cummer S. A. Measurement of a Broadband Negative Index with Space-Coiling Acoustic Metamaterials. *Physical Review Letters*, 2013, 110(17): 175501.
- [15] Qi Shuibao, Li Yong, and Assouar Badreddine. Acoustic Focusing and Energy Confinement Based on Multilateral Metasurfaces. *Physical Review Applied*, 2019, 7(5): 054006.
- [16] Zheng Bo, et al. High-Throughput Superresolved Focal Imaging Based on a Phase-Modulated Acoustic Superoscillatory Lens. *Physical Review Applied*, 2022, 18(1): 014048.
- [17] Li Yong, et al. Acoustic focusing by coiling up space. *Applied Physics Letters*, 2012, 101(23): 233508.
- [18] Li Yong, et al. Tunable Asymmetric Transmission via Lossy Acoustic Metasurfaces. *Physical Review Letters*, 2017, 119(3): 035501.
- [19] Wang Xu, Fang Xinsheng, Mao Dongxing, Jing Yun, and Li Yong. Extremely Asymmetrical Acoustic Metasurface Mirror at the Exceptional Point. *Physical Review Letters*, 2019, 123 (3): 214302.

- [20] Quan Li, Zhong Xu, Liu Xiaozhou, Gong Xiufen, and Johnson P. A. Effective impedance boundary optimization and its contribution to dipole radiation and radiation pattern control. *Nature Communications*, 2014, 5: 3188.
- [21] Cheng Ying, et al. Ultra-sparse metasurface for high reflection of low-frequency sound based on artificial Mie resonances. *Nature Materials*, 2015, 14: 1013-1019.
- [22] Zhu Xuefeng, Liang Bin, Kan Weiwei, Peng Yugui, and Cheng Jiangchun. Deep-Subwavelength-Scale Directional Sensing Based on Highly Localized Dipolar Mie Resonances. *Physical Review Applied*, 2016, 5(5): 054015.
- [23] Zhou Chen, Yuan Baoguo, Cheng Ying, and Liu Xiaojun. Precise rainbow trapping for low-frequency acoustic waves with micro Mie resonance-based structures. *Applied Physics Letters*, 2016, 108(6): 063501.
- [24] Zhang Jin, Cheng Ying, and Liu Xiaojun. Extraordinary acoustic transmission at low frequency by a tunable acoustic impedance metasurface based on coupled Mie resonators. *Applied Physics Letters*, 2017, 110(23): 233502.
- [25] Liu Chen, Long Houyou, Zhou Chen, Cheng Ying, and Liu Xiaojun. Reversed Doppler effect based on hybridized acoustic Mie resonances. *Scientific Reports*, 2020, 10: 1519.
- [26] Zhang Zhiwang, Cheng Ying, Liu Xiaojun, and Christensen Johan. Subwavelength multiple topological interface states in one-dimensional labyrinthine acoustic metamaterials. *Physical Review B*, 2019, 99(22): 224104.